Journal of
Analytical & Bioanalytical Techniques

Clifton Fagerquist and William Zaragoza, J Anal Bioanal Tech 2018, 9:2
DOI: 10.4172/2155-9872.1000400

Research Article Open Access

Possible Mistranslation of Shiga Toxin from Pathogenic *Escherichia coli* as Measured by MALDI-TOF and Orbitrap Mass Spectrometry

Clifton K. Fagerquist* and William J. Zaragoza

Produce Safety and Microbiology Research Unit, Western Regional Research Centre, Agricultural Research Service, US Department of Agriculture, 800 Buchanan Street, Albany, California 94710, USA

Abstract

Rationale: Shiga toxin-producing *Escherichia coli* (STEC) are often subjected to DNA damaging antibiotics during culturing in order to elicit the bacterial SOS response and up-regulation of bacteriophage-encoded proteins including Shiga toxin (Stx). However, such antibiotic exposure and stress may also have effects on protein expression.

Methods: *Escherichia coli* O157:H7 strain EDL933 was grown on Luria-Bertani agar (LBA) supplemented with a sub-inhibitory concentration of ciprofloxacin. Bacterial cells were harvested, suspended in water, gently vortexed and centrifuged. Supernatants were analyzed by MALDI-TOF and nano-LC-ESI-Orbitrap mass spectrometry. A gene knockout was constructed to delete the B-subunit gene from the stx_{2a} operon in the EDL933 strain.

Results: We detected the B-subunits of Stx1a and Stx2a and also peaks in close proximity to these B-subunits. The mass difference between these variants and the Stx1a B-subunit are: -43 Da, +16 Da and +54 Da. For Stx2a B-subunit, the mass differences are: -111 Da, -91 Da, -72 Da, -59 Da, -44 Da, -29 Da, -15/-17 Da, +16 Da, +32 Da, +53/54 Da, +106 Da. When the stx_{2a} gene knockout strain was cultured, it revealed the complete absence of the Stx2a B-subunit as well as its associated mass variants suggesting that the variants may be due to amino acid substitutions caused by translational errors.

Conclusions: Our results suggest that ciprofloxacin (a fluoroquinolone antibiotic) may cause translational errors in expression of Stx. Incorporation of mistranslated B-subunit sequences into the Stx AB_5 holotoxin has the potential to subtly alter its quaternary structure and its binding affinity to surface receptors of eukaryotic cells.

Keywords: *Escherichia coli*; Bacteriophage; Ciprofloxacin; Mass spectrometry

Introduction

Shiga toxin-producing *Escherichia coli* (STEC) are a significant public health risk worldwide [1]. The STEC outbreak from *E. coli* O104:H4 in Germany and France in 2011 quickly overwhelmed public health and healthcare organizations to identify and treat those afflicted [2,3]. Regulatory agencies also struggled to quickly and accurately identify the source of the STEC strain. As STEC outbreaks are almost entirely foodborne illnesses, it is critical for regulatory agencies to identify, test and recall (if necessary) suspected adulterated food commodities.

Major STEC outbreaks have also occurred in the USA as well as other countries over a number of years and even decades with *E. coli* O157:H7 being one of the most notable outbreak strains [4]. The natural host of STEC are the gastrointestinal tract (GI) of cattle which remain asymptomatic as they lack the Gb3 receptor necessary for recognition and binding of Shiga toxin [5]. However, STEC strains can spread during cattle transport and/or processing or by way of excreted feces that can contaminate the soil and water supply. Insects, birds and feral animals can also transmit STEC bacteria from cattle feces to agricultural fields whose finished products although extensively washed and refrigerated are not necessarily cooked prior to consumption.

Shiga toxin (Stx) itself is an AB_5 toxin that has five identical B-subunits that are non-covalently assembled into a donut-shaped structure that has five-fold symmetry. The catalytically active A-subunit is positioned on one side of the "donut" as well as a small part of the A-subunit (A2) that fits within the hole of the "donut" providing increased stability. The side opposite to that of the A-subunit binds to surface receptors of a cell. As such, it is the quaternary structure formed from the five B-subunits (and to some degree the A2 fragment) that provides the requisite surface epitope(s) for binding affinity and attachment to the cell surface receptors [6].

STEC infections present unique challenges with respect to patient treatment because many of the antibiotics used for treatment of a bacterial infection may inadvertently trigger the expression of *stx* genes and the release of Stx into the patient. The AB_5 Shiga holotoxin binds to surface receptors of eukaryotic cells: most importantly globotriaosylceramide (Gb3 and Gb4) receptors that are prevalent on kidney and other eukaryotic cells. Once attached to the cell surface, the holotoxin is enveloped by the cell after which it follows a retrograde pathway from the Golgi to the endoplasmic reticulum to the nucleus. Ultimately, the A-subunit of the holotoxin is enzymatically cleaved by proteases and released into the cytoplasm where it disables ribosomal protein synthesis leading to cell death [6].

Shiga toxin genes (stx_1 and stx_2) are located in bacteriophage (BP) genomes, and these BP genomes are transferred and lysogenized into

***Corresponding author:** Clifton K. Fagerquist, Produce Safety and Microbiology Research Unit, Western Regional Research Centre, Agricultural Research Service, US Department of Agriculture, 800 Buchanan Street, Albany, California 94710, USA, Tel: 5105595691; Fax: 5105596162; E-mail: clifton.fagerquist@ars.usda.gov

Received March 05, 2018; **Accepted** March 12, 2018; **Published** March 15, 2018

Citation: Clifton K. Fagerquist, William J. Zaragoza (2018) Possible Mistranslation of Shiga Toxin from Pathogenic *Escherichia coli* as Measured by MALDI-TOF and Orbitrap Mass Spectrometry. J Anal Bioanal Tech 9: 400. doi: 10.4172/2155-9872.1000400

bacterial host genomes by a process called horizontal or lateral gene transfer [7]. Expression of BP-encoded proteins (and Stx) occurs when the BP switches from its lysogenic cycle (a latent or dormant state in which BP DNA is replicated with host DNA) to the lytic cycle. The BP lysogenic/lytic switch is a consequence of a series of biological events in the bacterial host triggered by damage of its DNA, i.e., the SOS response [8]. Thus, some antibiotics, whose antimicrobial mode-of-action is to damage or disable bacterial DNA, e.g., by cross-linking DNA or inhibition of the replication fork, may also elicit a series of biological responses that lead to expression and release of Stx. In consequence, many antibiotics are contra-indicated for treatment of a suspected STEC infection.

A number of techniques have been developed to detect and characterize Stx from environmental and clinical isolates [9-13]. Monoclonal antibody (MAb)-based assays (e.g., ELISA, etc.) are very popular as (once developed and validated) they can be utilized in non-laboratory settings by end-users who require very little training or expertise in their use [10,11]. Another advantage is they can be used for screening a large number of samples. However, MAb-based approaches can also be plagued by non-specific binding especially for detection in complex matrices leading to false positives or a lack of detection. In addition, any initial positive result from such an assay must be considered *presumptive* until it is confirmed by another, typically orthogonal technique, i.e., bioassay or a chemical/physical-based technique such as mass spectrometry [9,12,13].

An additional complexity of Stx detection and identification is that an STEC strain may have multiple *stx* genes of different types and subtypes, e.g., *E. coli* O157:H7 strain EDL933 has stx_{1a} and stx_{2a} genes (both are expressed) [14,15]. PCR is often used to identify *stx* genes irrespective of whether the genes are actually expressed [16]. Clinical subtypes of Stx2 (a, c and d) require highly specific primers and thermocycler conditions that can discriminate between closely-related stx_2 genes. This can be challenging as a-, c- and d-subtypes represent a *continuum* of Stx2 subtypes, and a sharp dividing line between one clinical subtype and another is somewhat arbitrary [16].

Mass spectrometry and mass spectrometry-based proteomics provides high chemical and physical specificity of expressed proteins including Stx. STECs harboring single or multiple *stx* genes, e.g., *E. coli* O157:H7 strain EDL933 (stx_{1a} and stx_{2a}) [14,15] and *E. coli* O157:H- strain E32511 (stx_{2a} and stx_{2c}) [17], can be identified and distinguished by this technique if the toxin(s) are expressed. Expression of Stx from a putative STEC strain known to have (or suspected of having) a single or multiple *stx* gene(s) often requires specific culturing conditions (i.e., minimal media or exposure to specific antibiotics) that inhibit growth but also trigger a bacterial response leading to expression of BP-encoded proteins including Stx. Without such *induced* culturing conditions, the level of toxin expressed is often inadequate for detection from an unfractionated sample analyzed by MALDI-TOF-MS and MS/MS. We previously identified the B-subunit and A2 fragment (of the A-subunit) of Stx1a and Stx2a from *E. coli* O157:H7 strain EDL933 using MALDI-TOF-TOF mass spectrometry and top-down proteomic analysis [12,13,18].

In the current work, we have utilized MALDI-TOF-MS, nano-ESI-LC-Orbitrap mass spectrometry and molecular biology techniques to determine the origin of mass variants of B-subunits of Stx1a and Stx2a that appear when *E. coli* O157:H7 strain EDL933 is cultured on solid agar supplemented with ciprofloxacin antibiotic. Portions of this work were presented at the 65th Conference on Mass Spectrometry and Allied Topics (Indianapolis, IN June 4-8, 2017) [19].

Material and Methods

Bacterial strains, plasmids, and growth media

For routine culturing, strains were grown in Luria-Bertani broth (LBB) at 37°C. For strains containing temperature-sensitive plasmids, culturing was performed at 27°C to ensure replication of the plasmid. Antibiotic concentrations used were as follows: ampicillin (Amp) 100 μg mL^{-1} and kanomycin (Km) 50 μg mL^{-1}.

Polymerase chain reaction (PCR)

Primers used in this study are listed in Table 1. Linear and plasmid DNA was purified with either: Illustra GFX PCR DNA and gel band purification kit (GE Healthcare and Life Sciences, Catalogue Number: 28-9034-70), QIAamp DNA mini kit (Qiagen, Catalogue Number 51304) or QIAGEN Plasmid Mini Kit (Qiagen, Catalogue Number 12123) as appropriate. Amplification of the Km cassette with appended "arms" homologous to $stx_{2a\_B\text{-}subunit}$ from *E. coli* EDL933 was carried out on the pKD4 plasmid template using PFX Platinum Polymerase (Life Technologies, Catalogue Number 11708013) following manufacturer specifications. PCR was performed on a Tetrad 2 (Bio-Rad, Hercules, CA) with the following cycling conditions: 94°C for 5 min followed by 34 cycles of 94°C for 15 seconds, 55°C for 30 seconds, and 68°C for 2 min with a final elongation step at 68°C for 7 min. Confirmatory PCRs were carried out with Taq DNA polymerase (New England BioLabs, Catalogue Number M0273L) and PFX polymerase, respectively, with the following thermocycler conditions: 94°C for 5 min, followed by 29 cycles of 94°C for 30 sec, 53°C for 30 sec, 72°C for 2 min, followed by a final elongation step of 72°C for 7 min.

Transformations

Electroporations were performed with a Bio-Rad MicroPulser (Catalogue Number 165-2100) using sterile cuvettes with a 0.2 cm gap using the following protocol: host recipients were grown overnight in LBB at the appropriate temperature (27°C or 37°C) and sub-cultured in LBB the following day with the appropriate antibiotics to an optical density ($OD_{600\ nm}$) of 0.4. Cells were then chilled on ice for 10 min and 3 mL of sub-culture was pelleted via centrifugation at 3200 rpm for 10 min at 4 °C. Cells were then washed with ice-cold 10% glycerol and pelleted three times as above and re-suspended in ice-cold water to prepare them for electroporation. Then, 2 μg of DNA was mixed with 50 μL of cell suspension and placed in an ice-cold cuvette for electroporation. Following transformation, cells were quickly suspended in NZY recovery buffer (Fisher Scientific) with 2% glucose and incubated at either 37°C for one hour before being plated on the appropriate recovery media and incubated overnight. All transformants were confirmed by PCR and growth on selective media.

Construction of an EDL933 mutant: Δ$stx_{2a_B\text{-}subunit}$

The Km cassette was amplified from the pKD4 plasmid, generating a linear piece of DNA, using stx2aB_FP1 and stx2aB_RP1 primers in Table 1. These primers contain the Km cassette flanked by regions of homology (in bold) to the *E. coli* EDL933 $stx_{2a\_B\text{-}subunit}$ gene. This PCR product was excised from an agarose gel and purified with the GFX PCR DNA and gel band purification kit (as above). The result was transformed into *E. coli* strain EDL933 bearing plasmid pKD46 (courtesy of Maria Brandl, Ph.D., USDA ARS), resulting in the mutant strain WJZ21. The resulting transformants were plated on LB agar containing Km and confirmed by PCR for the insertion of Km resistance. The primers used for confirmation of deletion of stx2aB are also given in Table 1. Following confirmation of gene disruption, this

Primer	Oligonucleotide sequence (5'-3')	Additional Information
stx2aB_FP1	AGAAAGTCACAGTTTTTATATACAACGGGTAA ATAAAGGAGTTAAGCATGGTGTAGGCTGGAGCTGCTTC	Forward primer for amplifying the kanomycin casette from pKD4. Arms of homology to EDL933 are in bold
stx2aB_RP1	GACACAGATTACACTTGTTACCCACATACCAC GAATCAGGTTATGCCTCAATGGGAATTAGCCATGGTCC	Reverse primer for amplifying the kanomycin casette from pKD4. Arms of homology to EDL933 are in bold
stx2aB_ Conf_F	CAACGGGTAAATAAAGGAG	Forward primer for confirmation of deletion of stx2- B subunit
stx2aB_ Conf_R	CCCACATACCACGAATCA	Reverse primer for confirmation of deletion of stx2- B subunit

Table 1: The primers used for confirmation of deletion of stx2aB.

construct was then sub-cultured for multiple days at 37°C in order to cure the strain of the pKD46 plasmid.

MALDI-TOF mass spectrometry

Escherichia coli O157:H7 strain EDL933 and the $\Delta stx_{2a\_B\text{-}subunit}$ mutant strain (WJZ21) were grown overnight on Luria-Bertani agar (LBA) supplemented with a 20 ng/mL of ciprofloxacin [12,13]. Bacterial cells were harvested, suspended in water, gently vortexed and centrifuged so as to avoid cell lysis [18]. Supernatants were analyzed by MALDI-TOF-MS as previously detailed [12,13]. Briefly, a 0.5 µL aliquot was spotted onto a stainless steel target and allowed to dry. This dried sample spot was then over-layed with a saturated solution (33% acetonitrile, 67% water and 0.1% formic acid) of sinapinic acid (Protea Biosciences, Morgantown, WV) and also allowed to dry. The instrument utilized was a 4800 MALDI-TOF-TOF mass spectrometer (Sciex). Mass data was collected in linear mode. Prior to data collection, the linear mode was calibrated with a standard mixture of proteins: cytochrome-C, myoglobin and lysozyme all obtained from the same source (Sigma-Aldrich, St. Louis, MO).

Nano-liquid chromatography-electrospray ionization-orbitrap mass spectrometry

Sample supernatants were also analyzed using nano-LC-ESI-Orbitrap mass spectrometry (Velos Pro LTQ-Orbitrap, ThemoFisher, San Jose, CA). The splitless nano-HPLC system used was an ekspert™ nanoLC400 (Eksigent, AB Sciex, Redwood City, CA). A third pump was installed on this system to allow three separate (but simultaneous) functions upon three analytical columns, i.e., elution, washing and loading. This nano-HPLC system was interfaced to a multi-column PicoSlide platform (New Objective, Woburn, MA). The analytical column was a PicoChip HALO Protein (C4, 3.4 µm, 400 Å, 105 mm) operated at a flow rate of 400 nL/min.

Buffer A was 98% water, 2% acetonitrile and 0.1% formic acid. Buffer B was 100% acetonitrile and 0.1% formic acid. All solvents were Optima® LC/MS grade (Fisher Chemical). A 2.0 µL aliquot of sample from a snap-cap vial was loaded onto a 20 µL loop of the autosampler. Total elution time was 60 minutes. The elution gradient is as follows: Buffer B: 3% to 30% from t_0 to 15 min; 30% to 40% from 15 min to 45 min; 40% to 90% from 45 min to 53 min; 90% to 90% from 53 min to 57 min; 90% to 0% from 57 min to 60 min.

Nano-ESI was performed at 2.6 kV in positive ion mode. The eluent was at a flow rate of 400 nL/min. The heated stainless steel transfer line was set at 300°C. LC/MS data was collected at a resolution of 60,000 in FTMS profile mode using the Orbitrap mass analyzer. Mass-to-charge (*m/z*) range was 400-2000. All samples were analyzed in triplicate.

Results and Discussion

Figure 1A shows the MALDI-TOF-MS spectrum of *E. coli* O157:H7 strain EDL933 grown overnight on LBA supplemented with 20 ng/mL of ciprofloxacin. The B-subunit of Stx2a (Stx2a B-subunit) is the most prominent peak in the spectrum. The identity of this peak had been confirmed previously by MS/MS and top-down proteomic analysis [12]. Figure 1B shows an expanded mass-to-charge (*m/z*) range of the **1A** spectrum. From this expanded view, other peaks at *m/z* 7797 and 7773 appear either as a shoulder or nearby the highly intense Stx2a B-subunit peak. The peak at *m/z* 7691 was identified previously as the B-subunit of Stx1a by MS/MS and top-down proteomic analysis [18]. A MALDI matrix adduct of Stx2a B-subunit appears at *m/z* 8026 [20]. Figure 1C is a y-axis expansion (8%) of the 1B spectrum which allow a better view of less abundance peaks. The expanded view clearly shows discrete peaks adjacent to the very intense Stx2a B-subunit peak. In addition, a shoulder peak at *m/z* 7875 is also apparent. Culturing of this strain on LBA (no ciprofloxacin) results in no detection of Stx1a B-subunit or Stx2a B-subunit (or associated peaks), and the only proteins detected are bacterial host proteins [12,18].

It should be noted that it is easier to detect and distinguish a less abundant analyte that is close in *m/z* to an abundant analyte if the less abundant analyte is *lower* in *m/z*. The reason is that for TOF mass analyzers a less abundant analyte that has a lower *m/z* will strike the detector *prior* to the abundant analyte. A less abundant analyte that is *higher* in *m/z* to that of the abundant analyte may not be as easily distinguished because it strikes the detector *after* the abundant analyte. A certain amount of time is required for the signal generated by the detector (and associated electronics) to recover sufficiently to detect an ion packet of a weak abundant analyte that is trailing (in time) with respect to the ion packet of the abundant analyte. This issue is apparent when comparing peaks at *m/z* 7773 and 7875. The peak at *m/z* 7773 is more distinct than the peak at *m/z* 7875.

The peaks at *m/z* 7773 and 7797 were particularly intriguing as they appeared to correspond to the masses of other subtypes of Stx2, specifically Stx2c/d and Stx2g, respectively [16,21]. However, the genome of *E. coli* O157:H7 strain EDL933 has been exhaustively studied by multiple researchers and found to have only two Shiga toxin genes located separately in two bacteriophage genomes inserted into the bacterial host genome. stx_{1a} is located in a cryptic phage (CP-933V), and stx_{2a} is located in a prophage (BP-933W) [14,15]. In consequence, the additional peaks were due either to protein mistranslation or post-translational modifications (PTM). The PTMs of Stx have been well documented [6]. The full, translated B-subunit sequence undergoes removal of an N-terminal signal peptide, and this truncated, mature B-subunit sequence has one intramolecular disulfide bond [6].

We reasoned that deleting the gene of the Stx2a B-subunit from the EDL933 strain (a gene knockout) would help to clarify the origin of these additional peaks. Figure 2A shows the MALDI-TOF-MS spectrum of *E. coli* O157:H7 strain WJZ21 (a Δstx_{2a} of the B-subunit of *E. coli* O157:H7 strain EDL933) grown overnight on LBA supplemented with 20 ng/mL of ciprofloxacin. The B-subunit of Stx2a is now absent from the spectrum (as well as associated peaks) and the

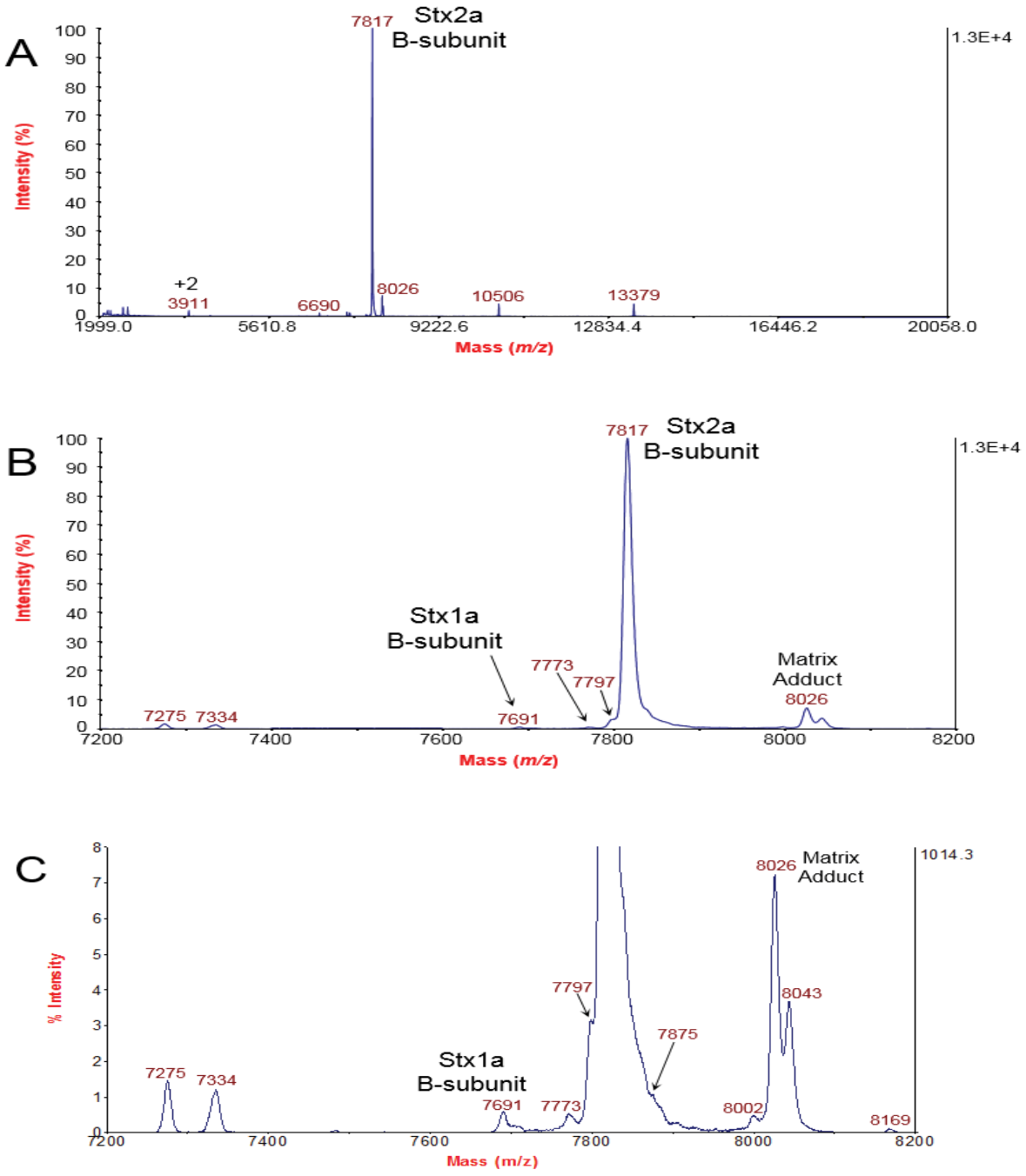

Figure 1: (A) shows the MALDI-TOF-MS spectrum of *E. coli* O157:H7 strain EDL933 grown overnight on LBA supplemented with 20 ng/mL of ciprofloxacin. **(B)** shows an expanded mass-to-charge (*m/z*) range. **(C)** shows a y-axis expansion (8%) of **1B** spectrum which allow a better view of less abundance peaks.

most abundant protein ion is an induced bacteriophage protein at *m/z* 13377 previously identified as an uncharacterized protein at locus tag 933Wp55 (synonym L0117) [18]. The peak at *m/z* 10507 was also previously identified as another uncharacterized bacteriophage protein: 933Wp74/L0136 [18]. The B-subunit of Stx1a is still detected at *m/z* 7693 as its gene was not deleted. Figure 2B shows an expanded *m/z* region that shows the complete absence of the B-subunit of Stx2a as well as the satellite peaks observed in Figure 1 including the matrix adduct peaks. Thus, the satellite peaks clustered around the Stx2a B-subunit peak in Figure 1 ultimately originate from the same B-subunit stx_{2a} gene. These results strongly suggest that these additional peaks (mass variants) are due to mistranslation of Shiga toxin caused by antibiotic induction.

Figure 3A shows the nano-LC/MS chromatogram of *E. coli* O157:H7 strain EDL933 grown overnight on LBA supplemented with 20 ng/mL of ciprofloxacin. The total ion chromatogram (TIC) and extracted ion chromatogram (XIC) of the +7 charge state of the

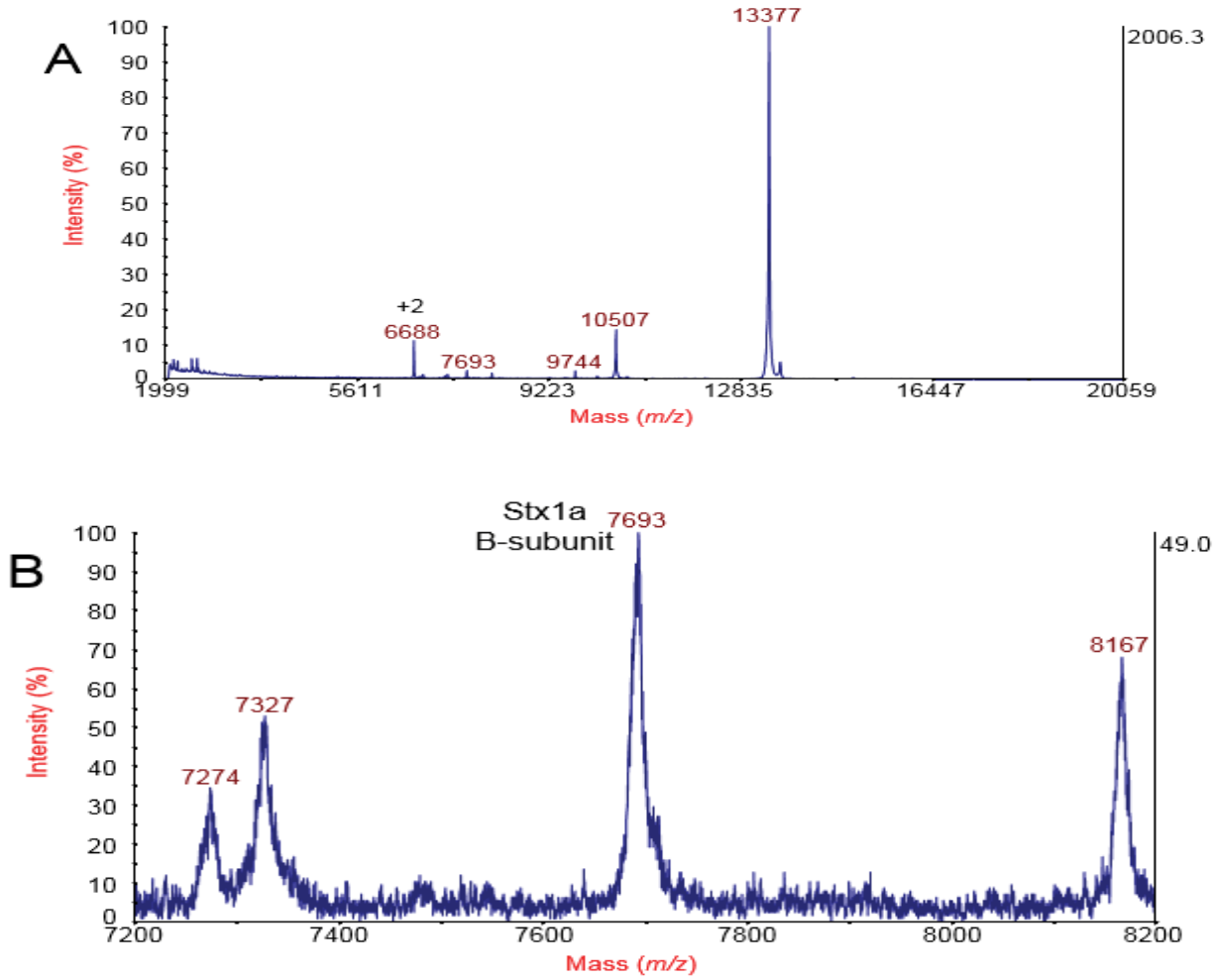

Figure 2: (A) shows the MALDI-TOF-MS spectrum of *E. coli* O157:H7 strain WJZ21 (a Δstx_{2a} of the B-subunit of *E. coli* O157:H7 strain EDL933) grown overnight on LBA supplemented with 20 ng/mL of ciprofloxacin. (**B)** shows an expanded *m/z* range.

B-subunit of Stx2a are presented. As can be seen, the Stx2a B-subunit elutes around 24 minutes but it also has a significant elution tail. In Figure 3B, MS scans are summed across a major portion of the Stx2a B-subunit peak (23.75 to 24.73 minutes) revealing a narrow charge state envelope from +5 to +8 with major ion intensity protein ions at +7 and +6 charge states. This is not surprising Stx2a B-subunit is a relatively small protein, and since its disulfide bond is intact, it has a lasso-loop secondary structure as opposed to a linear chain structure [22]. The mature sequence of Stx2a B-subunit is shown in Figure 3. The cysteine residues of the disulfide bond are underlined. It should be noted that there are seven basic residues (highlighted in red) whose side-chains can each accommodate one ionizable proton. These basic residues are all located within the "loop". An eighth possible protonation site is at the N-terminus which is only a few residues away from two lysine residues (**K**). It is likely that once seven protonation sites have been occupied, the effects of Coulomb repulsion would inhibit (although not entirely eliminate) an eighth protonation which would explain the steep drop in intensity from +7 to +8 charge states.

Figure 3C expands the *m/z* region around the +7 charge state of Stx2a B-subunit from Figure 3B. Just as in Figure 1, where minor satellite peaks are observed clustered around the +1 charge state of Stx2a B-subunit peak, a similar appearance of minor intensity peaks are clustered around the +7 charge state of Stx2a B-subunit (as well as +6 charge state). The greater sensitivity and resolution of nano-ESI-Orbitrap mass spectrometry allows identification of many more of these minor intensity peaks than is possible by MALDI-TOF. As shown these minor peaks are both higher (+16 Da, +32Da, +53/54 Da, +106 Da) and lower in mass (-44 Da, -15/-17 Da) than the mass of the Stx2a B-subunit peak. The Orbitrap detector allows detection of both lower *m/z* mass variants as well as higher *m/z* mass variants, i.e., the higher *m/z* mass variants no longer appear as indistinguishable shoulders on the strong Stx2a B-subunit ion signal unlike the MALDI-TOF data (Figure 1). The number of different mass variants detected would strongly argue against new, undiscovered PTMs. The most likely explanation is that a number of amino acid substitutions have occurred perhaps due to antibiotic-induced mistranslation resulting in a series of Stx mass variants. This is conclusion is supported by a comparison of the XIC of the +7 charge state of Stx2a B-subunit and the XIC of the +7 charge state of the mass variants shown in Supplemental Figure 1. With

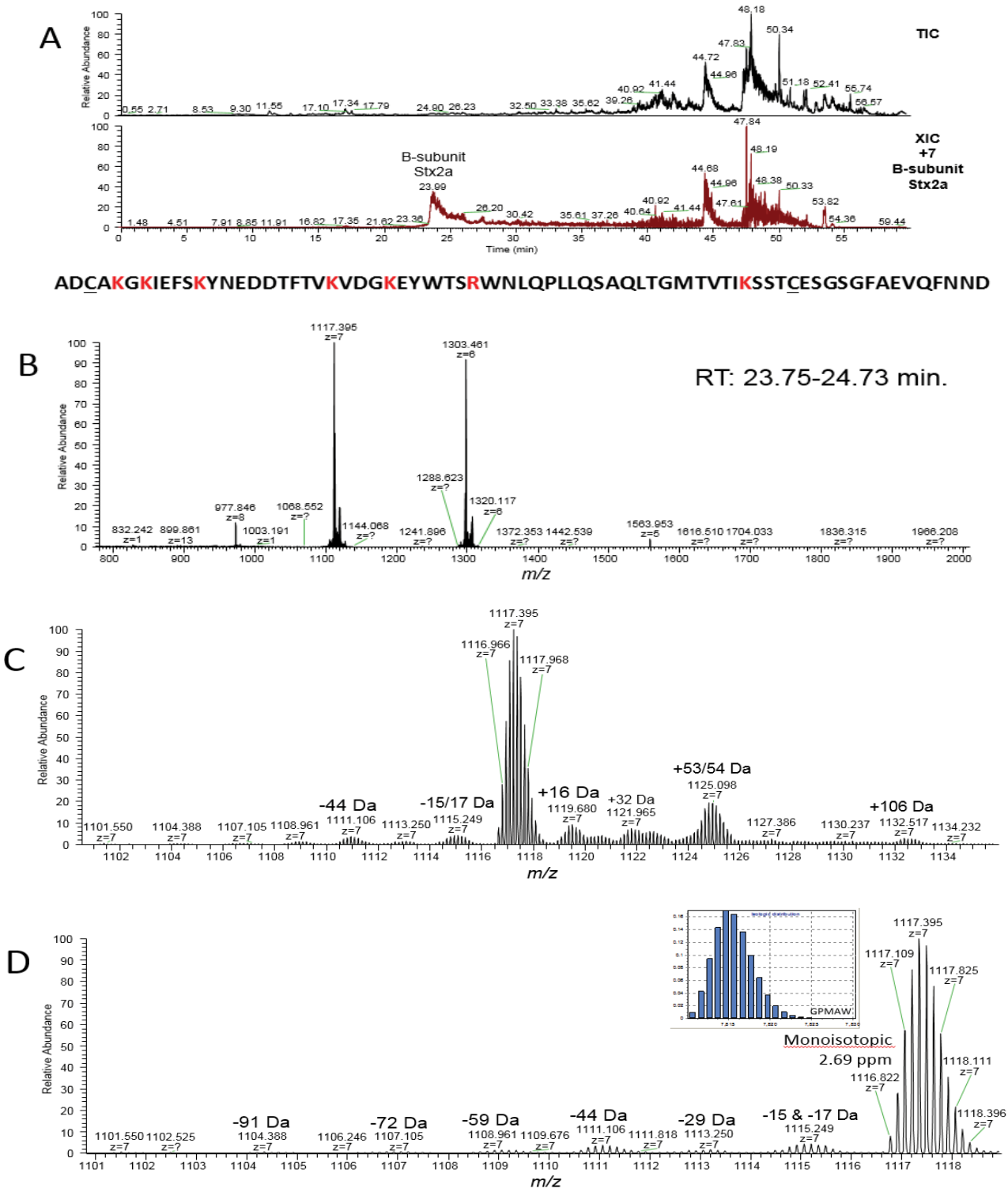

Figure 3: (A) shows the nano-LC/MS chromatogram of *E. coli* O157:H7 strain EDL933 grown overnight on LBA supplemented with 20 ng/mL of ciprofloxacin. The total ion chromatogram (TIC) and extracted ion chromatogram (XIC) of the +7 charge state of the Stx2a B-subunit are shown. The mature sequence of Stx2a B-subunit is shown below (basic residues in red and cysteine residues underlined). **(B)** shows the summed MS scans across the XIC LC peak (23.75 to 24.73 minutes) of Stx2a B-subunit. (**C)** expands the *m/z* range around the +7 charge state of Stx2a B-subunit of **3B**. (**D)** shows a further *m/z* expansion on the low *m/z* side of the Stx2a B-subunit. The insert shows the theoretical isotopic distribution of Stx2a B-subunit.

the possible exception of the +16 Da mass variant, the chromatograms of the mass variants closely correlate with the chromatogram of the Stx2a B-subunit suggesting that the chemical characteristics of these variants are not significantly different from that of the Stx2a B-subunit sequence.

A further *m/z* expansion on the low mass side of Stx2a B-subunit is shown in Figure 3D. A number of other mass variants are detected. The -44 Da mass variant is particularly interesting as it also appears clearly in Figure 1 at *m/z* 7773. The theoretical isotopic distribution of Stx2a B-subunit (as calculated by GPMAW) is shown as an insert. The observed and theoretical distributions are in excellent agreement. The mono-isotopic isotopomer of the +7 charge state of Stx2a B-subunit is observed at *m/z* 1116.822 which is in excellent agreement with its theoretical value of *m/z* 1116.819.

Figure 4A shows the previous TIC and XIC of the +7 charge state of Stx2a B-subunit as well as the XIC of the +7 charge state of Stx1a B-subunit. The Stx1a B-subunit peak elutes at 25.23 minutes somewhat later than Stx2a B-subunit and with significantly less tailing. As Stx1a B-subunit and Stx2a B-subunit sequences are similar but different (with 66.7% homology) [23], it is not surprising that they should have slightly different retention times. In Figure 4B, MS scans are summed across a major portion of the Stx1a B-subunit peak (24.97 to 25.54 minutes). Because of overlap in the retention time of Stx1a B-subunit and Stx2a B-subunit, we observe charge states of both. Interestingly, we also observe a subtle shifting in the relative intensities of charge states of Stx1a B-subunit and Stx2a B-subunit. The mature protein sequence of Stx1a B-subunit is shown in Figure 4. The cysteine residues of the disulfide bond are underlined. Like Stx2a B-subunit, it has seven basic residues (highlighted in red). However, unlike Stx2a B-subunit, not all the basic residues are located in the "loop" formed by the disulfide bond; one basic residue is located at the C-terminus. This would suggest that Stx1a B-subunit should be better able to accommodate eight ionizing protons than Stx2a B-subunit due to a lessening of Coulomb repulsion resulting from a series of more separated basic residues. This is observed experimentally with the more abundant Stx2a B-subunit being the dominant protein ion for the +5, +6 and +7 charge states compared to Stx1a B-subunit. However, for the +8 charge state a reversal occurs, and the Stx1a B-subunit ion is more intense than the Stx2a B-subunit ion. Coulomb repulsion is obviously having a significant effect on the relative intensity of Stx1a B-subunit and Stx2a B-subunit ions for the +8 charge state compared to its effect at lower charge states.

Figure 4C expands the *m/z* region around the +7 charge state of Stx1a and Stx2a B-subunits. A number of mass variants are observed for both Stx1a and Stx2a B-subunits. Like Stx2a B-subunit, Stx1a B-subunit has a mass variant at +54 Da and at -43 Da which would suggest that the amino acid substitutions responsible for these variants are common to both Stx sequences. Figure 4D is a further *m/z* expansion around the +7 charge state of Stx1a B-subunit showing all detectable isotopomers for this charge state. The mono-isotopic isotopomer *m/z* is 1098.692 which is in excellent agreement with the theoretical value of 1098.689. In addition, the observed isotopic distribution is also in excellent agreement with theoretical calculation (insert).

Figure 5A shows the nano-LC-MS chromatogram of *E. coli* O157:H7 strain WJZ21 (a Δstx_{2a} of the B-subunit of *E. coli* O157:H7 strain EDL933) grown overnight on LBA supplemented with 20 ng/mL of ciprofloxacin. The TIC and XIC of the +7 charge state of the B-subunit of Stx1a are presented. The retention time of the Stx1a B-subunit is only ~5 seconds different from that shown in Figure 4A. Figure 5B shows the sum of MS scans across this XIC peak from 25.13 to 25.62 minutes. Only the +6, +7 and +8 charge states of Stx1a B-subunit are observed. Stx2a B-subunit is not observed consistent with the results obtained by MALDI-TOF in Figure 2. Figure 5C shows an expansion in *m/z* around the +7 charge state reveals the +16 Da and +53 Da mass variants. Finally, Figure 5D shows the isotopic distribution of the +7 charge state. The mono-isotopic isotopomer is at *m/z* 1098.695 which is good agreement with the theoretical value of 1098.689. The isotopic distribution is also in good agreement with theory (insert).

-44 Da mass variant of Stx2a B-subunit

Assuming that a *single* amino acid substitution is responsible for the observed -44 Da mass variant, there are four possible substitutions for the Stx2a B-subunit sequence:

Thr → Gly	(Δm=44.02622 Da), seven possible sites
Asp → Ala	(Δm=43.98983 Da), five possible sites
Met → Ser	(Δm=44.00846 Da), one possible site
Phe → Cys	(Δm=44.05922 Da), four possible sites.

The mass difference (Δm), as calculated from the monoisotopic isotopomer of Stx2a B-subunit and the monoisotopic isotopomer of -44 Da mass variant, was performed for the +6 and +7 charge states for three LC-MS analyses. The average and standard deviation (Ave ± SD) of six Δm calculations was 44.016 ± 0.015 Da. On the basis of Δm, only Thr → Gly substitution or a Met → Ser substitution could account for the -44 Da mass variant. For a Thr → Gly substitution, there are *seven* possible sites in the Stx2a B-subunit sequence at which the substitution might occur. For a Met → Ser substitution, there is only *one* possible site for this to occur. If a Thr → Gly substitution is responsible for the -44 Da mass variant, given that there are seven potential sites for this substitution to occur, detection of a second Thr → Gly substitution may be expected, i.e., a -88 Da mass variant, however, a -88 Da mass variant was not detected (Supplemental Figure 2). Another possibility is that the -44 Da mass variant is the result of two amino acid substitutions, e.g., substitutions that result in the -29 Da mass variant and the -15 Da mass variant combined. Although such a scenario is possible, it would seem unlikely given the relative intensity of -44 Da, -29 Da and -15 Da mass variants.

The relative amount of the -44 Da mass variant can be calculated from the relative abundance of the Stx2a B-subunit peak versus the -44 Da mass variant peak from the MALDI-TOF and Orbitrap data. The integrated area of the peaks at *m/z* 7817 and *m/z* 7773 in the MALDI-TOF data of three technical replicates resulted in 0.0033 ± 0.0016 (Ave ± SD). Thus, as ionized and analyzed by MALDI-TOF from an *unfractionated* sample, the Stx2a B-subunit is about 300 times more abundant than the -44 Da mass variant. However, the Orbitrap results of the integrated peak areas from an LC fractionated sample for three technical replicates resulted in 0.040 ± 0.003 (Ave ± SD). Thus, the Stx2a B-subunit is about 25 times more abundant than the -44 Da mass variant. The response curve of the MALDI-TOF detector (multi-channel plate) may not be entirely linear with respect to the detection of a low abundant *versus* high abundant analyte. It is possible that the MALDI-TOF detector undercounts the less abundant -44 Da mass variant. In contrast, the Orbitrap detector, which detects image current, provides a better estimation of the relative abundance of these two analytes.

Possible translational errors Stx B-subunit expression

The codons for the two possible amino acid substitutions are shown

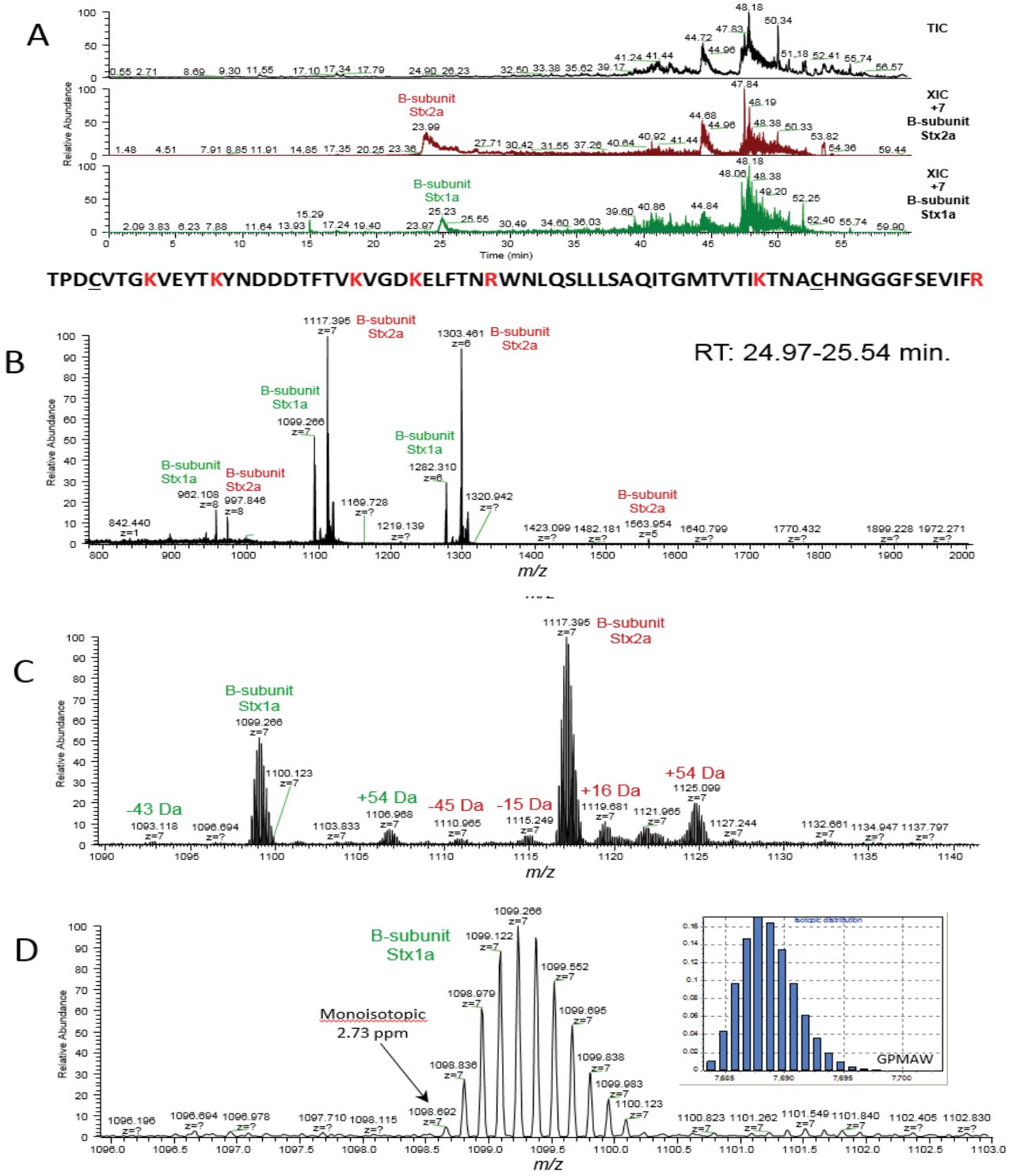

Figure 4: (A) shows the nano-LC/MS chromatogram of *E. coli* O157:H7 strain EDL933 grown overnight on LBA supplemented with 20 ng/mL of ciprofloxacin. The previous TIC and XIC of the +7 charge state of Stx2a B-subunit as well as the XIC of the +7 charge state of Stx1a B-subunit are both shown for purposes of comparison. The mature sequence of Stx1a B-subunit is shown below (basic residues in red and cysteine residues underlined). **(B)** shows the summed MS scans across the XIC LC peak (24.97 to 25.54 minutes) of Stx1a B-subunit. **(C)** expands the *m/z* range around the +7 charge state of Stx1a and Stx2a B-subunits from **4B**. **(D)** is a further *m/z* expansion around the +7 charge state of Stx1a B-subunit showing all detectable isotopomers of this charge state. The insert shows the theoretical isotopic distribution of Stx1a B-subunit.

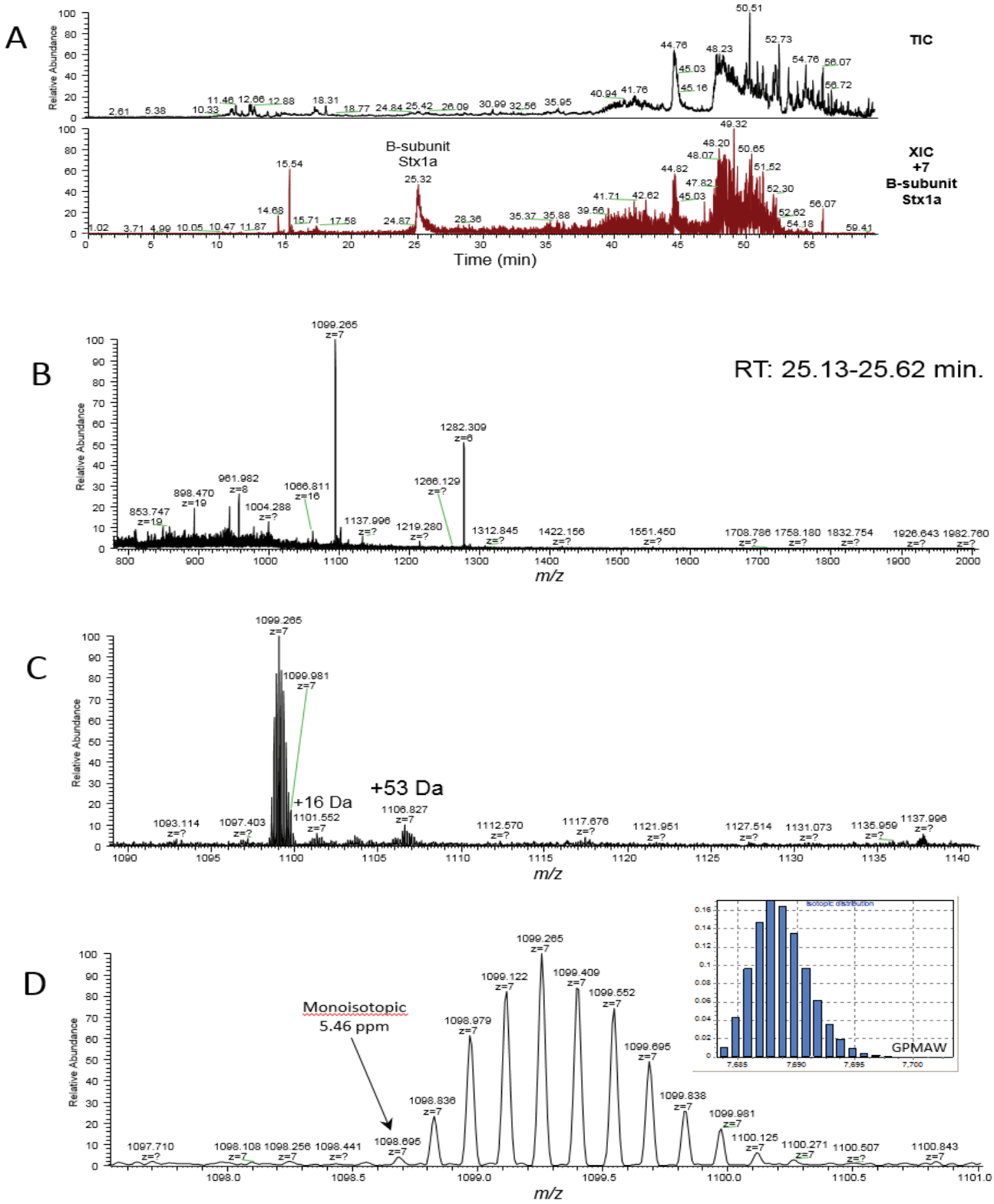

Figure 5: (A) shows the nano-LC/MS chromatogram of *E. coli* O157:H7 strain WJZ21 (a Δstx_{2a} of the B-subunit of *E. coli* O157:H7 strain EDL933) grown overnight on LBA supplemented with 20 ng/mL of ciprofloxacin. The TIC and XIC of the +7 charge state of the B-subunit of Stx1a are shown. **(B)** shows the summed MS scans across the XIC LC peak (25.13 to 25.62 minutes) of the Stx1a B-subunit. **(C)** expands *m/z* range around the +7 charge state showing all detectable isotopomers of this charge state. **(D)** shows a further expansion of *m/z* and an insert of the theoretical isotopic distribution of Stx1a B-subunit.

below. Codon bases that are identical and have the same position in the substitution pair are highlighted in red.

Thr (**ACA**, **ACC**, **ACG**, **ACU**) → Gly (**GGA**, **GGC**, **GGG**, **GGU**)

Met (**AUG**) → Ser (**AGC**, **AGU**, **UCA**, **UCC**, **UCG**, **UCU**)

For the Thr → Gly substitution, only the 3rd position (wobble position) is found to have any codon commonality. Met has only one codon: AUG. Its cognate $tRNA^{Met}$ anticodon is UAC. The anticodons of the first two $tRNA^{Ser}$ are UCG and UCA, respectively. A Met → Ser substitution involving the first two $tRNA^{Ser}$ anticodons would require a U•C codon-anticodon mismatch in the middle position as well as a G•G or a G•A mismatch in the wobble position (3rd position) [24]. In a series of detailed measurements on the stability of complementary (and near-complementary) anticodon-anticodon tRNA pairs, Grosjean et al. reported that when uridine (U) occupies the middle position of an anticodon, it can result in stable mismatches for U•U and U•G in the middle position as well as UU and U•C in the wobble position [25]. Unfortunately, there is no information on the stability of a U•C mismatch in the middle position.

Kramer and Farabaugh have noted previously that the rate of mistranslation of a particular amino acid is dependent on the concentration of its corresponding $tRNA^{AA}$ [26]. They also noted that since the rate constant for codon recognition is first order, and therefore dependent on the concentration of the specific $tRNA^{AA}$, i.e., a low abundant $tRNA^{AA}$ would result in an increase translational misreading of that specific residue [25,26]. If the abundance of a particular $tRNA^{AA}$ is low, the rate of its mistranslation would increase. Met is a not a particularly abundant amino acid in bacterial proteins aside from its critical role as the first residue of every protein. *E. coli* utilizes a non-canonical pathway for methionine biosynthesis not shared by many other bacteria [27]. It is possible that translation of BP-encoded proteins during the lytic cycle results in a deficit of $tRNA^{Met}$, and the single Met present in the mature B-subunit sequence of Stx2a is replaced with a Ser residue despite codon-anticodon mismatches in the middle and wobble positions. It is also possible that ciprofloxacin may facilitate misreading of the AUG codon. Kramer and Farabaugh have reported previously that aminoglycoside antibiotics can affect translational misreading for specific codons in *Escherichia coli* as well as in *Saccharomyces cerevisiae* [26,28].

Interestingly, the Stx1a B-subunit also has a single Met in the mature sequence, and we detect a -43/44 Da mass variant although its intensity is weaker due to the overall weaker expression of Stx1 (Figure 4). In addition, we have found evidence for this substitution for the Stx2c B-subunit subtype expressed in *E. coli* O157:H- strain E32511 when cultured on media supplemented with ciprofloxacin [17].

A number of researchers have reported evidence of translational misreading due to antibiotic exposure [26,29,30]. Kramer and Farabaugh reported mistranslation rates for lysine incorporation in *Escherichia coli* when exposed to the aminoglycoside antibiotics: streptomycin and paromycin [26]. They noted that the effect on translation error rates were far more specific for certain codons than initially realized. In other words, the antibiotic effect on codon misreading was not identical for all codons.

Ciprofloxacin has been found to trigger the SOS response (a bacterial DNA damage response) in STEC strains causing BP in the host bacteria to switch from their dormant lysogenic state to the lytic cycle. In turn, the lytic cycle results in expression of BP-encoded proteins including Stx whose genes are located in the BP genome that itself is located in the bacterial host genome. During the lytic cycle, the machinery of bacterial protein synthesis is co-opted by the BP to synthesize only its proteins. In consequence, evidence of translational errors caused by ciprofloxacin would logically be more apparent in BP-encoded proteins, e.g., Stx.

Conclusions

We have detected what appear to be amino acid substitutions in the B-subunits of Stx1a and Stx2a as a result of overnight culturing of *E. coli* O157:H7 strain EDL933 on solid agar supplemented with ciprofloxacin. The resulting B-subunit mass variants were detected by both MALDI-TOF and nano-LC-ESI-Orbitrap mass spectrometry. A gene knockout of the B-subunit of Stx2a confirmed that the mass variants originated from the stx_{2a} gene. As all the PTMs of B-subunit of Stx are known, i.e., signal peptide removal and an intramolecular disulfide bond, the number of mass variants detected suggest amino acid substitutions resulting perhaps from antibiotic-induced mistranslation during protein synthesis.

On the basis of high resolution monoisotopic analysis, a -44 Da mass variant of the Stx2a B-subunit may result from substitution of the only Met residue in the mature protein sequence with a Ser residue. Another possibility is Thr → Gly, however as there are *seven* potential sites for this substitution to occur, one would expect to observe multiple Thr → Gly substitutions (i.e., -88 Da mass variant). As no -88 Da mass variant was observed, it suggests that Met → Ser is the most likely substitution for the -44 Da mass variant. Stx1a B-subunit exhibited a similar -44 Da mass variant and also has a single Met in its mature sequence.

Detection of Stx B-subunit mass variants is important for a number of reasons. First, certain masses of the Stx2a B-subunit variants initially suggested "new" Stx subtypes in this already highly studied STEC strain. However, careful review of this strain indicated only stx_{1a} and stx_{2a} genes as being present. A stx_{2a} gene knockout of the B-subunit confirmed that the observed mass variants were due to the original stx_{2a} gene. Second, Stx mistranslation could result in the incorporation of these protein sequences into the AB_5 holotoxin resulting in subtle changes of its quaternary structure that may affect its binding to eukaryotic cell receptors such as globotriaosylceramide (Gb3). Third, monoclonal antibody-based diagnostic assays used for detecting and/or typing of Stx may be similarly affected by the incorporation of these mistranslated sequences into the holotoxin possibly resulting in erroneous or confusing results.

Although evidence for antibiotic-induced mistranslation in bacteria has been reported by previous researchers, there is little information on the effect of ciprofloxacin (or other fluoroquinolones) on this phenomenon.

Acknowledgments

This research was supported by USDA-ARS CRIS project 5325-42000-051-00D.

References

1. Karmali MA (2017) Emerging Public Health Challenges of Shiga Toxin-Producing *Escherichia coli* Related to Changes in the Pathogen, the Population, and the Environment. Clin Infect Dis 64: 371-376.
2. Fruth A, Prager R, Tietze E, Rabsch W, Flieger A (2015) Molecular epidemiological view on Shiga toxin-producing *Escherichia coli* causing human disease in Germany: Diversity, prevalence, and outbreaks. Int J Med Microbiol 305: 697-704.
3. Navarro-Garcia F (2014) *Escherichia coli* O104:H4 Pathogenesis: an Enteroaggregative *E. coli*/Shiga Toxin-Producing *E. coli* Explosive Cocktail of High Virulence. Microbiol Spectr 2: 6.

4. Kulasekara BR, Jacobs M, Zhou Y, Wu Z, Sims E, et al. (2009) Analysis of the genome of the *Escherichia coli* O157:H7 2006 spinach-associated outbreak isolate indicates candidate genes that may enhance virulence. Infect Immun 77: 3713-3721.

5. Pruimboom-Brees IM, Morgan TW, Ackermann MR, Nystrom ED, Samuel JE, et al. (2000) Cattle lack vascular receptors for Escherichia coli O157:H7 Shiga toxins. Proc Natl Acad Sci USA 97: 10325-10329.

6. Johannes L, Römer W (2010) Shiga toxins--from cell biology to biomedical applications. Nat Rev Microbiol 8: 105-116.

7. Gillings MR (2017) Lateral gene transfer, bacterial genome evolution, and the Anthropocene. Ann NY Acad Sci 1389: 20-36.

8. Michel B (2005) After 30 Years of Study, the Bacterial SOS Response Still Surprises Us. PLoS Biology 3: e255.

9. Quiñones B, Swimley MS (2011) Use of a Vero cell-based fluorescent assay to assess relative toxicities of Shiga toxin 2 subtypes from *Escherichia coli*. Methods Mol Biol 739: 61-71.

10. Gehring AG, Fratamico PM, Lee J, Ruth L, He X, et al. (2017) Evaluation of ELISA tests specific for Shiga toxin 1 and 2 in food and water samples. Food Control 77: 145-149.

11. Wang J, Katani R, Li L, Hegde N, Roberts EL, et al. (2016) Rapid Detection of *Escherichia coli* O157 and Shiga Toxins by Lateral Flow Immunoassays. Toxins (Basel) 8: 92.

12. Fagerquist CK, Sultan O (2011) Induction and identification of disulfide-intact and disulfide-reduced β-subunit of Shiga toxin 2 from *Escherichia coli* O157:H7 using MALDI-TOF-TOF-MS/MS and top-down proteomics. Analyst 136: 1739-1746.

13. Fagerquist CK, Sultan O (2010) Top-down proteomic identification of furin-cleaved α-subunit of Shiga toxin 2 from *Escherichia coli* O157:H7 using MALDI-TOF-TOF-MS/MS. J Biomed Biotechnol, Article ID: 123460.

14. Latif H, Li HJ, Charusanti P, Palsson BØ, Aziz RK (2014) A Gapless, Unambiguous Genome Sequence of the Enterohemorrhagic *Escherichia coli* O157:H7 Strain EDL933. Genome Announc 2: 821-814.

15. Perna NT, Plunkett G 3rd, Burland V, Mau B, Glasner JD, et al. (2001) Genome sequence of enterohaemorrhagic *Escherichia coli* O157:H7. Nature 409: 529-533.

16. Scheutz F, Teel LD, Beutin L, Piérard D, Buvens G, et al. (2012) Multicenter evaluation of a sequence-based protocol for subtyping Shiga toxins and standardizing Stx nomenclature. J Clin Microbiol 50: 2951-2963.

17. Fagerquist CK, Zaragoza WJ (2015) Shiga toxin 2 subtypes of enterohemorrhagic *E. coli* O157:H- E32511 analyzed by RT-qPCR and top-down proteomics using MALDI-TOF-TOF-MS. J Am Soc Mass Spectrom 26: 788-799.

18. Fagerquist CK, Zaragoza WJ (2016) Bacteriophage cell lysis of Shiga toxin-producing *Escherichia coli* for top-down proteomic identification of Shiga toxins 1 and 2 using matrix-assisted laser desorption/ionization tandem time-of-flight mass spectrometry. Rapid Commun Mass Spectrom 30: 671-680.

19. Fagerquist CK, Zaragoza WJ (2017) Translational errors in expression of Shiga toxin from pathogenic *Escherichia coli* as measured by MALDI-TOF-TOF and Orbitrap mass spectrometry. 65th Conference on Mass Spectrometry and Allied Topics in Indianapolis, pp: 4-8.

20. Fagerquist CK, Sultan O, Carter MQ (2012) Possible evidence of amide bond formation between sinapinic acid and lysine-containing bacterial proteins by matrix-assisted laser desorption/ionization (MALDI) at 355 nm. J Am Soc Mass Spectrom 23: 2102-2014.

21. Fagerquist CK, Zaragoza WJ, Sultan O, Woo N, Quiñones B, et al. (2014) Top-down proteomic identification of Shiga toxin 2 subtypes from Shiga toxin-producing *Escherichia coli* by matrix-assisted laser desorption ionization-tandem time of flight mass spectrometry. Appl Environ Microbiol 80: 2928-2940.

22. Fraser ME, Fujinaga M, Cherney MM, Melton-Celsa AR, Twiddy EM, et al. (2004) Structure of shiga toxin type 2 (Stx2) from *Escherichia coli* O157:H7. J Biol Chem 279: 27511-27517.

23. Huang X, Miller W (1991) A time-efficient, linear-space local similarity algorithm. Adv Applied Math 12: 337-357.

24. Manickam N, Nag N, Abbasi A, Patel K, Farabaugh PJ (2014) Studies of translational misreading *in vivo* show that the ribosome very efficiently discriminates against most potential errors. RNA 20: 9-15.

25. Grosjean HJ, de Henau S, Crothers DM (1978) On the physical basis for ambiguity in genetic coding interactions. Proc Natl Acad Sci USA 75: 610-614.

26. Kramer EB, Farabaugh PJ (2007) The frequency of translational misreading errors in *E. coli* is largely determined by tRNA competition. RNA 13: 87-96.

27. Ferla MP, Patrick WM (2014) Bacterial methionine biosynthesis. Microbiology 160: 1571-1584.

28. Kramer EB, Vallabhaneni H, Mayer LM, Farabaugh PJ (2010) A comprehensive analysis of translational missense errors in the yeast *Saccharomyces cerevisiae*. RNA 16: 1797-1808.

29. Gorini L, Nomura M, Tissieres A, Lengyel P (1974) Cold Spring Harbor Laboratory. Cold Spring Harbor, NY, USA, pp: 791-804.

30. Kurland C, Hughes D, Ehrenberg M (1996) Limitations of translational accuracy. In *Escherichia coli* and *Salmonella*: cellular and molecular biology. ASM Press, Washington, DC, pp: 979-1004.